An abiotically catalyzed glucose fuel cell for powering medical implants: Reconstructed manufacturing protocol and analysis of performance

S. Kerzenmacher [a,*], J. Ducrée [b], R. Zengerle [a,b], F. von Stetten [a]

[a] Laboratory for MEMS Applications, Department of Microsystems Engineering (IMTEK), University of Freiburg, Georges-Koehler-Allee 106, D-79110 Freiburg, Germany
[b] HSG-IMIT, Wilhelm-Schickard-Strasse 10, D-78052 Villingen-Schwenningen, Germany

ARTICLE INFO

ABSTRACT

Although the first abiotically catalyzed glucose fuel cells have already been developed as sustainable power supply for medical implants in the 1970s, no detailed information concerning the fabrication of these devices has been published so far. Here we present a comprehensive manufacturing protocol for such a fuel cell, together with a detailed analysis of long-term performance in neutral buffer containing physiological amounts of glucose and oxygen. In air saturated solution a power density of $(3.3 \pm 0.2)\,\mu W\,cm^{-2}$ is displayed after 10 days of operation that gradually decreases to a value of $(1.0 \pm 0.05)\,\mu W\,cm^{-2}$ in the course of 224 days. A novelty of this work is the characterization of fuel cell performance with individually resolved electrode potentials. Using this technique, we can show that the major part of performance degradation originates from a positive shift of the anode potential, indicating that a more poisoning-resistant glucose oxidation catalyst would improve the degradation behavior of the fuel cell. As further factors influencing performance an incomplete reactant separation and a mass transfer governed cathode reaction under the relatively low oxygen partial pressures of body tissue have been identified. Consequently we propose an oxygen depleting electrode interlayer and the application of more effective oxygen reduction catalysts as promising strategies to further improve the fuel cell performance under physiological concentrations of glucose and oxygen.

© 2008 Elsevier B.V. All rights reserved.

1. Introduction

1.1. A sustainable fuel cell power supply for medical implants

At present, a number of approaches are being pursued to realize a battery-independent power supply for active medical implants [1,2]. Besides mechanical [3,4] and thermoelectric [5,6] generators, also implantable glucose fuel cells [7–9] are being considered. These fuel cells generate electrical energy by the electrochemical reaction of glucose with oxygen at two spatially separated electrodes. The relatively constant availability of glucose and oxygen in body fluids (e.g. blood, interstitial fluid) allows for the continuous production of electricity. This is their main advantage over mechanical and thermoelectric generators, both being dependent on the non-continuous nature of vibrations or temperature differences within the human body.

Key components in the design of glucose fuel cells are the active materials that catalyze the electrode reactions of glucose and oxygen. Whereas enzymatic catalysts offer high reactant specificity and high reaction rate, the limited stability of enzymes makes long-term operation difficult. The life-span of such fuel cells is typically in the order of weeks [10]. In the medical context such systems are currently only considered for the electricity supply of short-term implantable sensors [9,11]. An alternative option is the use of abiotic catalysts, as for instance platinum and activated carbon. These catalysts are less specific and exhibit generally lower reaction rates compared to enzymes, but their stability makes them preferable when it comes to long-term application.

The first prototype of an abiotically catalyzed glucose fuel cell as potential power supply for medical implants has been reported by Warner and Robinson [12]. Driven by the limited performance of implant batteries available at that time, a number of academic and industrial research groups actively pursued the technology during the following years [13–15]. In first *in vivo* studies [13,16], prototypes implanted subcutaneously in a dog exhibited power densities in the range of $2\,\mu W\,cm^{-2}$, which is sufficient to power a cardiac pacemaker, over periods of up to 5 months. Despite these promising results, the development has been stopped after the introduction of lithium–iodine batteries in 1972 [17–19] and the associated increase in the battery-dependent lifetime of cardiac pacemakers.

---

* Corresponding author. Tel.: +49 761 203 7328; fax: +49 761 203 7322.
E-mail address: sven.kerzenmacher@imtek.de (S. Kerzenmacher).

In the recent years two trends have revived the interest in abiotically catalyzed glucose fuel cells. On one side the lack of a truly sustainable implant power supply becomes more and more evident with the increasing number of low power MEMS (micro-electro-mechanical systems) implants [2]. At the same time there has been considerable progress in designing power efficient implant electronics, for example low power pacemaker circuits [20] or highly efficient bionic ear processors [21]. The applicability of abiotically catalyzed glucose fuel cells is thus no longer concentrated on cardiac pacemakers, but appears feasible for a wider range of implantable devices.

1.2. Manufacturing protocols and long-term performance studies in the literature

Although the general design and performance of abiotically catalyzed glucose fuel cells has been described in the literature before [13,15,22], the published information concerning manufacturing protocols and also performance characterization is inconclusive. Presumably due to the strong industry involvement, proprietary knowledge has often not been disclosed. An extensive literature review covering the available construction and performance data has been prepared by our group [23].

As key components the fabrication of the fuel cell electrodes is of particular interest. Whereas also commercially available platinum black fuel cell electrodes have been used [15,24], Rao et al. described the fabrication of electrodes from activated carbon with a glucose permeable polymer hydrogel as binder [14,22]. Similarly, Gebhardt et al. [25] reported the fabrication of self-supporting Raney-type electrodes for glucose oxidation from platinum–nickel alloy foils. Unfortunately the experimental procedures are not described in detail, rendering the reproduction of the historic work difficult.

In summary, a limitation of all literature reports is the lack of a comprehensive work that links a defined fabrication procedure to fuel cell performance. Furthermore, the long-term functionality of the historic devices has only been reported in terms of overall performance. A detailed investigation of the degradation behavior of the individual electrodes, pre-requisite for specific optimization, has to our best knowledge not yet been carried out. In the present work we address both issues by presenting a complete manufacturing procedure reconstructed from the available literature data of Rao et al. [14,16,22,26,27], together with the long-term *in vitro* performance of the anode and cathode over a period of 240 days. In addition the sensitivity of fuel cell performance to a variation of glucose and oxygen concentrations within the physiological range is investigated.

In Section 2 of this paper the general design and the selection of fuel cell materials are described, whereas the reconstructed manufacturing protocol is presented in Section 3. Section 4 comprises the experimental procedures for fuel cell characterization and data analysis, followed by the results and discussion part in Section 5 and a final conclusion.

2. Design of an abiotically catalyzed glucose fuel cell

For application as an implantable power supply, the fuel cell reconstructed in this work has to meet a number of requirements. Of utmost importance is the selection of potentially biocompatible materials that are amenable to established sterilization techniques, e.g. heat sterilization at 121 °C. To facilitate implantation and system integration, a surface mountable fuel cell would be desirable that operates in tissue rather than directly in the blood stream. Such a device can be implemented as an external coating to medical implants and would allow for the construction of a fully integrated

system, without the need for additional surgery and intra-body wire connections. Based on these requirements we identified the design originally reported by Rao et al. [14] as a promising approach for the reconstruction of a manufacturing protocol. In first animal trials their fuel cell showed encouraging results, exhibiting power densities of 1.6 μW cm^{-2} over a period of 150 days [16].

In the following sections the deduced reactant separation concept as well as the fuel cell construction materials used in this work are described and compared to the original design.

2.1. Reactant separation concept

With conventional fuel cells it is common to supply the reactants separately to the electrodes. This is not possible for a fuel cell operating in equilibrium with physiological fluid (e.g. interstitial fluid, blood), where both, oxygen and glucose, are dissolved. Catalysts for the selective reduction of oxygen in the presence of glucose are known, e.g. silver or activated carbon [26]. However, no non-enzymatic catalyst is presently available that allows for the selective glucose electro-oxidation in the presence of oxygen. On the surface of a noble metal catalyst both, glucose oxidation and oxygen reduction can therefore take place simultaneously. As a consequence the anode attains a mixed potential between the potentials of glucose oxidation and oxygen reduction. The terminal voltage of the fuel cell is thus drastically lowered, impairing the generation of electricity.

In order to circumvent this electrochemical short-circuit, we selected a variant of the electrode arrangement originally proposed by Rao et al. [28]. The reactant mixture diffuses from the surrounding environment into the fuel cell. Oxygen is selectively reduced at the outer *oxygen-selective cathode* (e.g. activated carbon, silver) and thus removed from the reactant mixture. This results in a predominantly anoxic region inside the fuel cell. There the electro-oxidation of glucose can take place at a non-selective platinum anode. The fuel cell can be mounted on an impermeable surface, since reactant access from one side is sufficient (Fig. 1). Both electrodes are fabricated from electrically conductive catalyst particles embedded in a glucose permeable polymer hydrogel binder. A separator membrane that allows for the diffusion of glucose and oxygen electrically insulates the electrodes.

Although this two-electrode setup is described in a patent by Rao et al. [29], performance data is only available for a version with a *central anode* arranged between *two* cathodes. This has to be considered when comparing the power density of their devices to the fuel cell described in this work.

2.2. Selection of fuel cell materials

The fuel cell materials used in this work are compared to the materials reported in historic works [14,16,22,26,27] in Table 1. As Rao et al. we used activated carbon as cathode catalyst, whereas our anode catalyst consisted of an activated carbon supported platinum–bismuth alloy. This catalyst is commercially available and has been specifically developed for the direct oxidation of glucose to gluconic acid [31]. From the various reported binders for electrode fabrication we selected a poly(vinyl alcohol)–poly(acrylic acid) hydrogel (PVA–PAA) since it can be easily crosslinked by thermal esterification. Instead of the originally reported silver mesh we employ a current collector made from platinum mesh, due to its chemical inertness and biocompatibility. As glucose permeable separator membrane between the electrodes, a commercially available, sterilizable polyethersulfone filter membrane has been chosen. To replace the original epoxy casing, a jet-cut polycarbonate frame was designed as structural support in which the fuel cell components are clamped together between silicone rubber gaskets
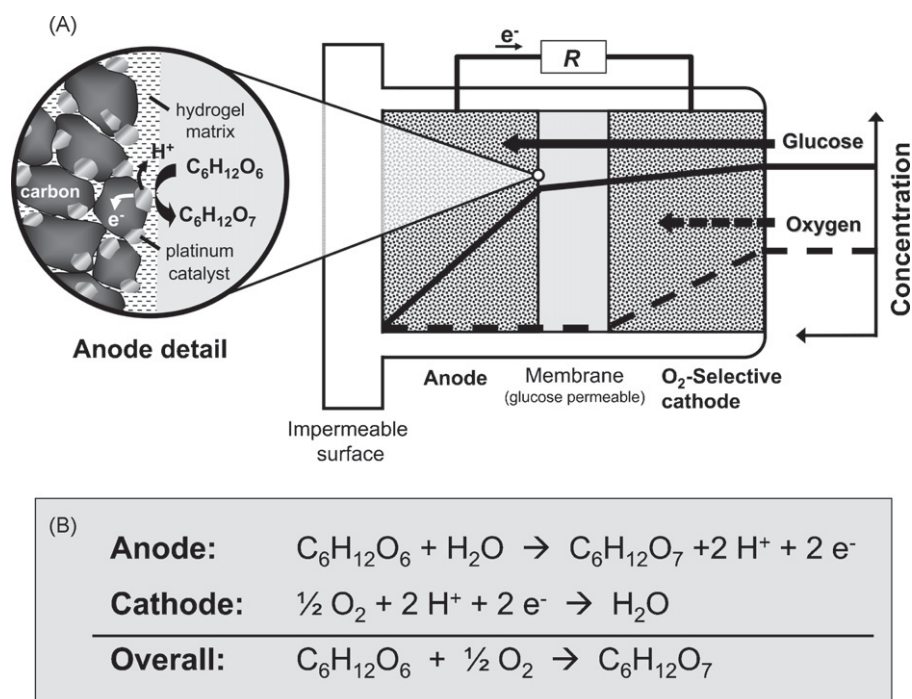
Fig. 1. (A) Reactant separation with oxygen-selective cathode catalyst and surface mountable electrode arrangement (after [28]). See text for explanations. (B) Principal electrode reactions of an abiotically catalyzed glucose fuel, assuming that glucose ($C_6H_{12}O_6$) is oxidized to gluconic acid ($C_6H_{12}O_7$) as the main reaction product (after [30]).

(Fig. 3). The frame allows for a rapid and versatile assembly of fuel cells for lab experiments. All fuel cell materials used in the present work have been chosen to be sterilizable and at least potentially biocompatible or non-toxic. Carbon and platinum [32] as well as PVA-based hydrogels [33,34] possess an established record of biocompatibility. Similarly, the polyethersulfone filter membrane has passed the *in vivo Biological Reactivity Test* according to USP Chapter 88 (Supor 450 product data sheet, Pall Corp., Ann Arbor, MI). A dedicated biocompatibility study for bismuth is – to our best knowledge – not available, yet. However, bismuth compounds have found wide use in the pharmaceutical field [35] and can thus be assumed to be non-toxic.

3. Reconstructed manufacturing protocol

The manufacturing of a complete fuel cell starts from a current collector that is impregnated with catalyst ink to form the individual electrodes. Together with a glucose permeable separator membrane the electrodes are then clamped together in a polycarbonate frame that gives structural support to the whole assembly. In the following section the individual manufacturing steps and materials are described in detail.

3.1. Current collector preparation

Plain weave platinum mesh (82 wires per inch, 60 μm wire diameter, Goodfellow, Bad Nauheim, Germany) with the dimensions 1.6 cm × 2.0 cm was cleaned with acetone and annealed for 30 min at 700 °C in air atmosphere to release internal stress from the fabrication process. A thin and stable structure was obtained by subsequent flattening of the mesh with a hydraulic press at approx. 20 kN cm^{-2}. Each current collector is fitted with two platinum wires to separately connect electrode voltage and current. To this end a 2.5 mm × 20 mm portion at the outer edge of the mesh was folded and two separate leads made from doubly twisted 50 μm platinum wire (Chempur, Karlsruhe, Germany) were introduced into the pocket. The electrical connection between the mesh and the wire was established by pressing the junction at approx. 40 kN cm^{-2}. To ensure a robust connection over the long-term experiment the junction was additionally protected by conductive carbon cement (Leit-C, Plano, Wetzlar, Germany).

3.2. Catalyst ink preparation

As catalyst material for the cathode activated carbon (A 196, Degussa AG Hanau, Germany) was used. The anode catalyst con-

Table 1
Comparison of the fuel cell construction materials

Fuel cell component	Rao et al.	This work
Oxygen reduction catalyst	Activated carbon [14]; silver [22]	Activated carbon
Glucose oxidation catalyst	Platinized activated carbon [14]; platinum black [26]; Pt–Ni alloy foil [25]	Activated carbon with 5% Pt + 5% Bi
Polymer binder	PVA–PAA (8:1 w/w) [14]; glycolmethacrylate [14]; methacrylic acid [22]	PVA–PAA (8:1 w/w)
Electrode thickness	Cathode: 250 μm [27]	480 μm
Separator membrane	PVA–PAA membrane [22]; PVA-soaked cellulose membranes, 20 μm [26]; sulfonated PTFE [22]; dialysis tubing [22]; cuprophane [22]	Hydrophilic polyethersulfone membrane with 450 nm pores, 140 μm thick
Current collector	Silver mesh [14]	Platinum mesh
Cell housing	Silastic [16]; epoxy resin [14]	Polycarbonate frame with silicone rubber gaskets

Table 2
Composition of the catalyst inks for cathode and anode

Component	Cathode composition (wt.%)	Anode composition (wt.%)
Activated carbon (A 196)	28.41	–
Activated carbon (CF 196, 5% Pt + 5% Bi)	–	30.77
PVA ($M \sim 240 \, kg \, mol^{-1}$)	4.18	4.06
PAA ($M \sim 205 \, kg \, mol^{-1}$)	0.52	0.51
H_2O	66.89	64.66

sisted of an activated carbon supported Pt–Bi alloy (CF 196, 5% Pt + 5% Bi, Degussa AG Hanau, Germany). Prior to weighing both materials were dried for 30 min at 110 °C under air. A spreadable catalyst ink was prepared by thoroughly mixing the catalyst powders with a solution prepared from distilled water and appropriate amounts of poly(vinyl alcohol) (PVA 40–88, $M \sim 205 \, kg \, mol^{-1}$, Fluka Chemie GmbH, Buchs, Switzerland) and poly(acrylic acid) (PAA, $M \sim 240 \, kg \, mol^{-1}$, 25 wt.% partial sodium salt in water, Aldrich Chem. Co., Milwaukee, WI). The exact composition of the inks is listed in Table 2. Air bubbles entrapped in the catalyst ink were removed by 10-min vacuum treatment at approx. 10 mbar.

3.3. Electrode fabrication

Electrodes were fabricated in a two-step process with a doctor blade technique, as illustrated in Fig. 2. A fluorinated ethylene propylene foil (FEP, Bohlender GmbH, Germany) served as substrate from which the dried electrodes could be easily removed. At first a layer of catalyst ink was spread to a thickness of 260 μm. The thickness of the layer was controlled by the height of a casting frame made from an appropriate number of adhesive tape layers. The platinum mesh current collector was introduced on top of the still wet catalyst layer. Immediately a second 260 μm layer of catalyst ink was applied with the same technique as before. The electrodes were dried overnight at room temperature and subsequently thermally crosslinked in air atmosphere at 145 °C for 80 min. The crosslinked electrodes and the polyethersulfone separator membrane (Pall Supor 450, 450 nm pore size, 140 μm thickness, VWR, Darmstadt, Germany) were equilibrated in phosphate buffered saline (PBS tabs/pH 7.4, Invitrogen, Karlsruhe, Germany) at room temperature. Entrapped air within the components was removed by a 60-min vacuum treatment in PBS at approx. 10 mbar.

3.4. Fuel cell assembly

Following the degassing step the still wet fuel cell components were clamped together in a polycarbonate holder (jet-cut from 5 mm Makrolon, Bayer Sheet Europe GmbH, Darmstadt, Germany), using silicone rubber gaskets (jet-cut from 2 mm thick silicone elastomer foil, # 115–2325, VWR, Darmstadt, Germany) and four nylon screws (Fig. 3). The complete device was immersed in PBS and subject to a second vacuum treatment to remove any air pockets that formed during the assembly procedure. Fig. 3 depicts the construction of the complete fuel cell. Both cathode and anode have a nominal thickness of 480 μm, with active electrode dimensions of 1.5 cm × 1.5 cm.

4. Experimental procedures

The long-term performance of three fuel cells has been characterized in a series of regularly recorded current density–potential curves. To avoid an overestimation of the performance by an excessively fast scan rate the current density has been increased in steps of $4.4 \, \mu A \, cm^{-2}$ once the fuel cells attained a stable potential with a voltage drift of less than $0.2 \, mV \, h^{-1}$. The recording of a complete load curve with seven current density steps thus requires approx. 1 week. Given the time-dependent degradation of the fuel cell performance it is not feasible to investigate the effect of different oxygen partial pressures on fuel cell performance by a sequential experimental procedure. The three fuel cells from the long-term experiment therefore serve as a baseline to which the performance of a fourth cell, operated in parallel but under different oxygen partial pressures, is compared. A different strategy has been devised to characterize the glucose sensitivity of the fuel cell performance. The fuel cells were operated at constant current density, and by stepwise additions of glucose its direct effect on electrode potential and thus fuel cell performance can be shown. In the following the test setup and the experimental procedures for long-term performance, oxygen sensitivity and glucose sensitivity as well as the data analysis are explained in detail.

4.1. Test setup

The fuel cells were mounted on top of a glass slide in individual 600 ml glass beakers using epoxy resin (UHU plus sofort fest, UHU Bühl, Germany). A polycarbonate (5 mm Makrolon, Bayer Sheet Europe GmbH, Darmstadt, Germany) lid with openings for aeration, medium exchange, reference electrode and gas outlet was fitted on top of the beaker and sealed with silicone elastomer (Sylgard 186, Dow Corning, Wiesbaden, Germany). It was also used to glue a 2-mm silicone rubber sheet with central hole on top of the polycarbonate lid. This way a gas-tight seal around the reference electrode opening could be established. All other openings were equipped with sterile filters (FP 30/0.2 CA-S, 0.2 μm pore size, Whatman GmbH, Dassel, Germany).

After assembly in the glass beakers the cells were autoclaved at 121 °C for 15 min in phosphate buffered saline to prevent the growth of microorganisms. The heat sensitive reference electrodes were thoroughly rinsed with 70 vol.% ethanol and introduced into the beakers after autoclavation under a sterile workbench. Subsequently the phosphate buffered saline was exchanged through the sterile filters with fresh, non-autoclaved phosphate buffered saline.

The individual fuel cells were connected in series with a single Keithley 2400 source meter (Keithley Instruments, Germering, Germany) operating in galvanostatic mode (at defined current), as depicted in Fig. 4. All fuel cells were therefore subject to an identical load profile throughout the experiments reported in this work. The potentials of cathode and anode were recorded in 5-min intervals against the saturated calomel reference electrode (KE11, Sensortechnik, Meinsberg, Germany), using a Keithley 2700 digital multimeter system (Keithley Instruments, Germering, Germany). In addition, for each data point the current was recorded by measuring the voltage drop across a 100 Ω shunt resistor connected in series with the fuel cells.

The aeration gas flow rate was controlled for each cell individually with a variable area flowmeter (Dwyer TMF-RMA-3-SSV,
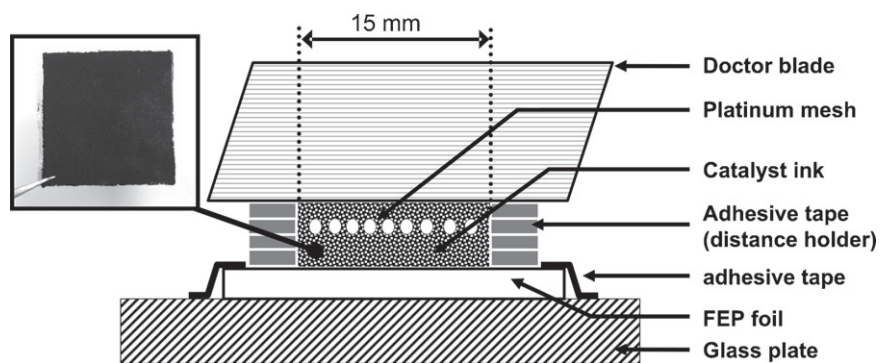
Fig. 2. Electrode fabrication by doctor blade technique. See Section 3.2 for explanations.
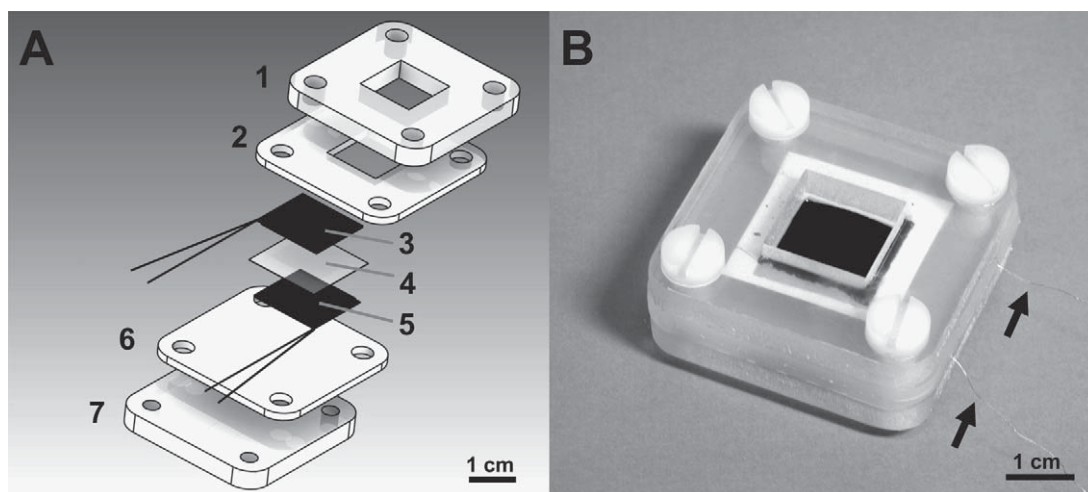

Fig. 3. (A) Fuel cell components. (1) Polycarbonate frame; (2) silicone rubber gasket; (3) cathode; (4) separator membrane; (5) anode; (6) silicone rubber gasket; (7) polycarbonate backing. (B) Picture of the prototype, the arrows indicate the wire connections.
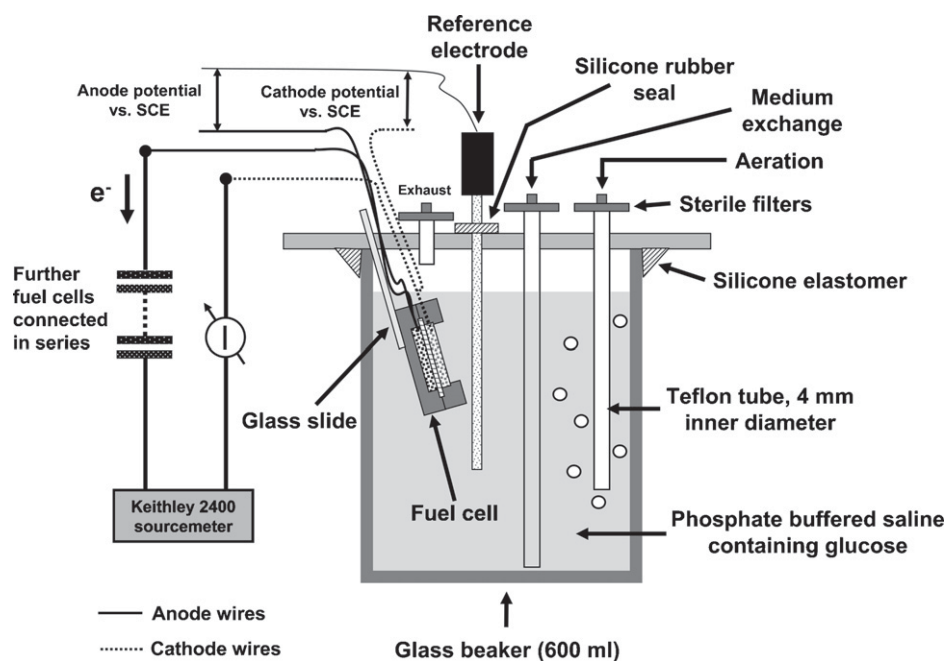

Fig. 4. Fuel cell test setup. See Section 4.1 for explanations.

Techmark, München, Germany) at $0.5\,L\,min^{-1}$. Excessive evaporation of the testing medium was prevented by humidification of the gases in a bubble column. Evaporated water was regularly replaced with distilled water through the sterile filters, the replenished volume typically amounting to less than 5% of the total volume. The complete setup was installed in an incubator to maintain the testing solution at a constant temperature of $(37 \pm 1)\,°C$.

4.2. Fuel cell start-up and long-term performance

For start-up the fuel cells were held at open circuit in fully aerated (pO_2 = 196 mbar), glucose-free PBS. After reaching a stable cell voltage the glucose concentration in testing solution was adjusted to $5.0 \times 10^{-3}\,mol\,L^{-1}$ by adding the appropriate amount of glucose (from α-D(+)-glucose monohydrate, Roth, Karlsruhe, Germany) dissolved in 5 ml distilled water through the sterile filter. Again, the fuel cells were allowed to reach a stable open circuit voltage (OCV), and then operated for 4 days at a current density of $17.8\,\mu A\,cm^{-2}$.

The long-term performance was characterized by performing seven load experiments over a period of 240 days. Starting from $0\,\mu A\,cm^{-2}$ (open circuit) to a maximum value of $26.7\,\mu A\,cm^{-2}$ the current density was increased in steps of $4.4\,\mu A\,cm^{-2}$ once all fuel cells reached a stable cell potential (voltage drift of less than $0.2\,mV\,h^{-1}$ at a given current density). The testing medium throughout this experiment was fully aerated (pO_2 = 196 mbar) PBS at $(37 \pm 1)\,°C$, containing $5.0 \times 10^{-3}\,mol\,L^{-1}$ glucose. Before each load experiment it was exchanged through the sterile filters.

In the final load experiment the testing medium was purged with nitrogen to remove oxygen. The anodes were operated against an external counter electrode and a load experiment was performed as described above while the fuel cell cathodes were held at open circuit. The counter electrode (platinum mesh) was situated in a separate beaker filled with PBS. Both beakers were connected by an ion bridge, constructed from a polymer wick inside a silicon rubber tube, filled with PBS.

In between 112 and 169 days of operation the fuel cells were operated at constant current density but under varying concentrations of glucose and oxygen, to investigate the glucose sensitivity of the fuel cells (see Section 4.4).

4.3. Oxygen sensitivity

In parallel to the long-term experiment a fourth fuel cell was operated under the same conditions but varying oxygen partial pressures. Between 30 and 80 days of operation complete load curves were obtained under oxygen partial pressures of 131, 65, and 33 mbar. Here, the oxygen partial pressure of 65 mbar (~7% oxygen saturation) is approximately between the values reported for well-vascularized tissue (38 mmHg [36]) and subcutaneous tissue of the human arm (60 mmHg [37]). In lack of more accurate data, this intermediate value was chosen as the upper limit resembling the physiological range in body tissue. As lower limit an oxygen partial pressure of 33 mbar (~3.5% oxygen saturation) was selected, which corresponds to the value found in the femoral muscle of the mouse (24 mmHg [38]). The oxygen concentration in the testing medium was adjusted by mixing corresponding amounts of nitrogen (99.999% purity) and air with variable area flowmeters (Model 112-02TA, Analyt-MTC, Müllheim, Germany; estimated accuracy: ± 2 mbar in terms of oxygen partial pressure). The total gas flow was kept constant at $0.5\,L\,min^{-1}$ in all cases.

4.4. Glucose sensitivity

To assess their glucose sensitivity the fuel cells were operated at constant current density but varying glucose concentrations

between 2.5×10^{-3} and $10.1 \times 10^{-3}\,mol\,L^{-1}$. This range includes the values reported for adipose tissue and blood (3.8×10^{-3} and $5.0 \times 10^{-3}\,mol\,L^{-1}$, respectively [39]). The glucose concentration was increased in steps of $1.3 \times 10^{-3}\,mol\,L^{-1}$ once the cell potential stabilized (voltage drift less than $0.2\,mV\,h^{-1}$). To maintain sterility the appropriate amounts of glucose were dissolved in 5 ml of distilled water and introduced into the beaker through a sterile filter. These experiments were performed at oxygen partial pressures of 196 mbar (corresponding to full aeration) and 33 mbar (corresponding to the low value of the estimated physiological range, see Section 4.3).

4.5. Data evaluation and graphical presentation

For each load experiment current density–potential plots were constructed from the stable (voltage drift less than $0.2\,mV\,h^{-1}$) electrode potentials at a given current.

The oxygen sensitivity of the fuel cells is presented in a graph showing the difference in electrode potential between three reference fuel cells (operated at pO_2 = 196 mbar) and a fourth fuel cell operated at lower oxygen partial pressures. Corresponding current density–potential difference plots were constructed according to the relation $\Delta E_{O_2} = E(O_2) - E_{Ref}$. Herein ΔE_{O_2} represents the difference in electrode potential, whereas $E(O_2)$ and E_{Ref} are the current density dependent electrode potentials of the fuel cells operated at lower oxygen partial pressure and the reference fuel cells, respectively.

A glucose sensitivity graph was constructed according to $\Delta E_{Glc} = E_{after} - E_{before}$. Here ΔE_{Glc} is the shift in anode potential, with E_{before} and E_{after} denoting the stable (voltage drift less than $0.2\,mV\,h^{-1}$) anode potential before and after increasing the glucose concentration in steps of $1.3 \times 10^{-3}\,mol\,L^{-1}$.

Throughout this work the experimental results for power density and potential are reported as (mean value $\pm$ sample standard deviation). Bars in graphs represent the minimum and maximum value of three experiments conducted in parallel.

5. Results and discussion

5.1. Fuel cell start-up

In Fig. 5 the exemplary start-up of one fuel cell in phosphate buffered saline at 37 °C is shown. Starting from time zero the test-
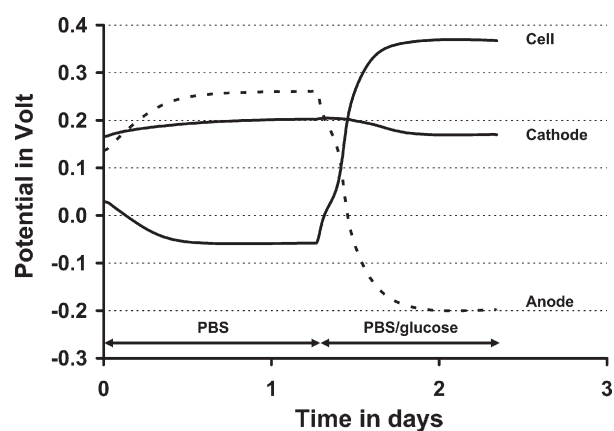

Fig. 5. Exemplary evolution of the electrode potentials at zero current (OCV) in PBS. Starting from time zero the testing solution was continuously bubbled with humid air, corresponding to an oxygen partial pressure of 196 mbar. After reaching a stable open circuit potential glucose was added, the final concentration amounting to $5.0 \times 10^{-3}\,mol\,L^{-1}$ glucose (as indicated in the figure).
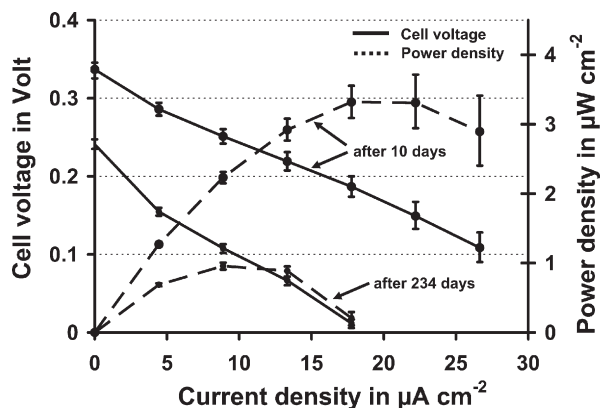
Fig. 6. Current density–potential plots of the complete fuel cells recorded after 10 and 234 days of operation, as indicated in the figure. Given are the average values of three parallel experiments, bars represent maximum and minimum values.

Fig. 8. Time-dependent evolution of cathode and anode potentials at open circuit (—), at $8.9\,\mu A\,cm^{-2}$ (– – –), and at $17.8\,\mu A\,cm^{-2}$ (- - -). Cathode and anode potentials (as indicated in the figure) are extracted from repeatedly recorded current density–potential plots and quoted against a saturated calomel electrode (SCE) in the same solution. Given is the average of three parallel experiments, bars represent maximum and minimum values.

ing solution was purged with humid air (pO_2 = 196 mbar). In the absence of glucose both fuel cell electrodes approach their respective open circuit potential of oxygen reduction within 1 day. Due to the higher catalytic activity of the platinum–bismuth catalyst the anode open circuit potential is by approximately 60 mV more positive than the open circuit potential of the activated carbon cathode, resulting in a reversal of cell polarity. Since platinum–bismuth is also catalytically active for glucose oxidation the anode open circuit potential attains a drastically more negative value upon addition of glucose to the testing solution. Due to the presence of oxygen and the associated mixed potential formation the open circuit potential of the anodes reaches only to $-(197 \pm 7)$ mV vs. SCE, in contrast to the $-(518 \pm 25)$ mV vs. SCE that have been obtained with similar electrodes in oxygen-free solution ([8], see also Fig. 9). The activated carbon cathode, which is not catalytically active towards glucose oxidation, exhibits only a small negative shift of approx. -20 mV in open circuit potential upon addition of glucose. The open circuit voltage of the complete fuel cells thus approaches (363 ± 11) mV.

5.2. Long-term performance

The average current density–potential curve of three glucose fuel cells, recorded after 10 days and again after 234 days of operation, is compared in Fig. 6. Its shape exhibits the typical fuel cell features. In the low current density range, between open circuit and $4.4\,\mu A\,cm^{-2}$, the slope of the voltage curve is steeper, correspond-
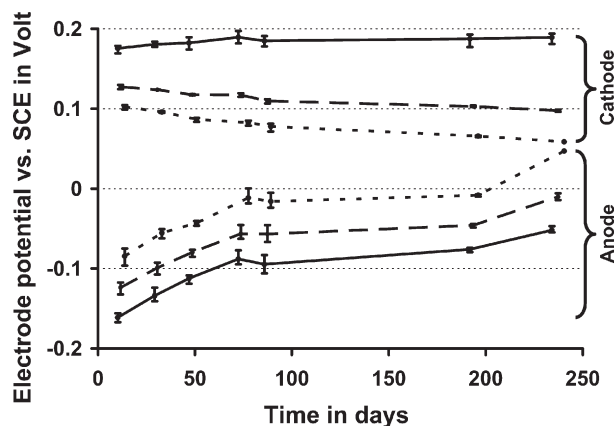
ing to the activation polarization of the electrochemical reactions [40]. At current densities between 4.4 and $13.9\,\mu A\,cm^{-2}$ the linear slope reflects the polarization attributed to ohmic losses within the fuel cell [40]. Over the investigated current density range no mass transport limitation is apparent, which would be indicated by a rapid decay of cell voltage at high current densities.

Between days 10 and 234 the maximum power density decreases from (3.3 ± 0.2) to $(1.0 \pm 0.05)\,\mu W\,cm^{-2}$, a reduction in performance by approx. 70%. This is comparable to the results of Rao et al. [22] where over a period of 80 days the power output of a fuel cell operated in modified Ringer-solution ($5 \times 10^{-3}\,mol\,L^{-1}$ glucose, pO_2 = 47 mbar) decreased by 50% from approx. 110 to 55 μW. Unfortunately the dimensions and construction of this fuel cell have not been specified, so that a direct comparison of power densities is not possible. Elsewhere Rao et al. reported power densities between 4 [14] and $7\,\mu W\,cm^{-2}$ [22], which is in the range of the present results.

From the polarization curves in Fig. 6 it is apparent that the performance degradation over time is largely caused by a loss in open circuit voltage, which decreases from (337 ± 10) mV at day 10 to (241 ± 6) mV at day 234. Only a minor fraction of the overall degradation stems from an increase in activation and also ohmic polarization. Here the performance characterization with
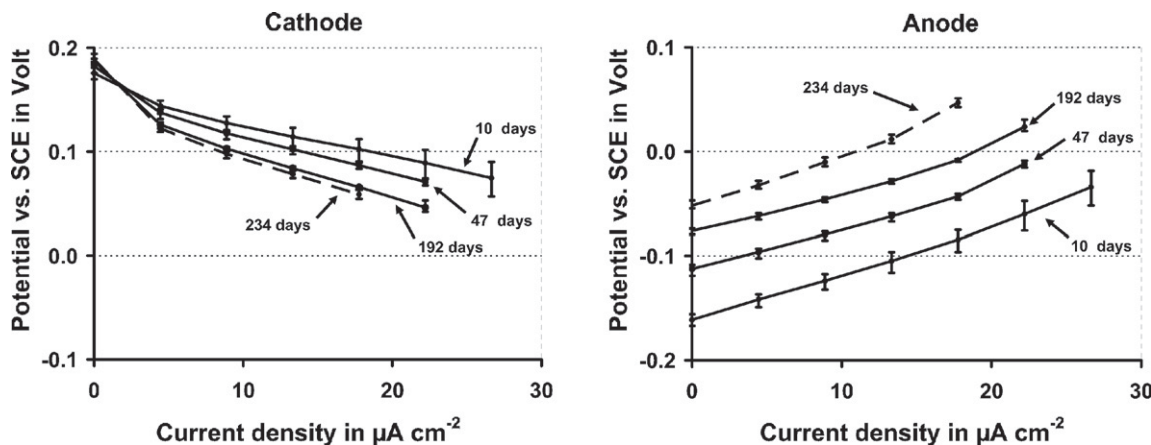

Fig. 7. Polarization plots of the fuel cell's cathode and anode, recorded after 10, 47, 192, and 234 days of operation (as indicated in the figure). Given is the average of three parallel experiments, bars represent maximum and minimum values.
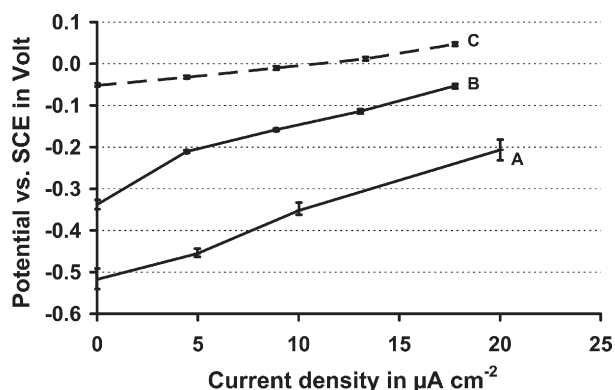
Fig. 9. Comparison between current density–potential plots of aged and freshly prepared anodes. (A) Freshly prepared half-cell anodes in oxygen-free solution. (B) Aged fuel cells anodes in oxygen-free solution (after 259 days of operation). (C) Aged fuel cells anodes in aerated solution (after 234 days of operation, see also Fig. 7). Given is the average of three parallel experiments, bars represent maximum and minimum values.

individually recorded electrode potentials allows for the separate assessment of cathode and anode degradation. The corresponding current density–potential plots, recorded at different times during the long-term experiment, are shown in Fig. 7. For clarity only the curves recorded after 10, 47, 192, and 234 days are displayed. In addition, the progression of performance degradation over the 240-day testing period is shown in Fig. 8. Displayed are the potentials of cathode and anode at open circuit, 4.4, and 17.8 $\mu A\,cm^{-2}$.

The cathode open circuit potential does not change significantly over the complete testing period. However, there is a gradual increase in cathode polarization under load. The degradation rate is virtually constant and amounts to $-(0.132 \pm 0.01)$ and $-(0.193 \pm 0.02)\,mV\,day^{-1}$ for current densities of 8.9 and 17.8 $\mu A\,cm^{-2}$, respectively (Fig. 8). From the shape of the cathode current density–potential plots degradation can be attributed to two processes, dominating in different current density regimes. At current densities below 4.4 $\mu A\,cm^{-2}$ the increased polarization suggests a decrease in catalytic activity of the catalyst (activation polarization). The area specific resistance of the cathode in the ohmic range can be calculated from the linear slope between 4.4 and 13.3 $\mu A\,cm^{-2}$. Between days 10 and 234 it increases from (75.4 ± 0.2) to $(111.2 \pm 3.8)\,k\Omega\,cm^2$. This suggests a decrease in electrical conductivity of the cathode due to a loss of electrical contact between the catalyst particles, and might be related to extended

swelling or chemical degradation (hydrolysis) of the PVA–PAA hydrogel binder [22].

A different behavior is observed at the anode, which clearly dominates the overall degradation of fuel cell performance. Between days 10 and 84 of the experiment the anode exhibits a higher degradation rate than the cathode. It amounts to $+(0.9 \pm 0.2)$ and $+(0.9 \pm 0.3)\,mV\,day^{-1}$ for current densities of 8.9 and 17.8 $\mu A\,cm^{-2}$, respectively. For both current densities this value decreases to $+(0.1 \pm 0.1)\,mV\,day^{-1}$ between 84 and 192 days of operation, which is comparable to the cathode. Although this suggests a possible stabilization there is again an increase in degradation rate between days 192 and 234 of the experiment, amounting to $+(0.8 \pm 0.1)$ and $+(1.2 \pm 0.1)\,mV\,day^{-1}$ for current densities of 8.9 and 17.8 $\mu A\,cm^{-2}$, respectively (Fig. 8).

As can be seen from both, Figs. 7 and 8, the anode degradation is governed by a large positive shift in open circuit potential, amounting to $+(109 \pm 10)\,mV$ between days 10 and 234. In contrast to the cathodes, the anode polarization plots exhibit a comparable slope throughout the experiment. Unfortunately, the linear slope between 4.4 and 13.3 $\mu A\,cm^{-2}$ cannot be solely attributed to ohmic anode polarization, due to the possible interference of oxygen crossover through the cathode. Therefore the calculation of the area specific resistance is not useful.

Although the positive shift in anode open circuit potential indicates a decrease in catalytic activity, a corresponding activation polarization in the low current density range is not observed. A reasonable explanation can be the presence of oxygen at the anode due to an incomplete reactant separation. The simultaneous oxidation of glucose and reduction of oxygen at the non-selective anode would thus lead to an internal current and polarization independent of external current flow. To verify this hypothesis the aged fuel cell anodes were operated in oxygen-free medium against an external counter electrode. The corresponding current density–potential plot, recorded after 259 days of operation is shown in Fig. 9, together with the polarization curve of freshly prepared similarly constructed half-cell anodes [8] in oxygen-free solution. For comparison, the current density–potential plot of the aged anodes operated as part of a fuel cell in aerated solution is also shown. The before mentioned hypothesis is endorsed by the experimental results, since in oxygen-free medium the aged fuel cell anodes now exhibit a pronounced activation polarization in the low current density region. In contrast, no activation polarization is apparent with the freshly prepared half-cell anodes operated under the same conditions. Furthermore, the open circuit potential of the aged anodes is by approximately 180 mV more positive than with
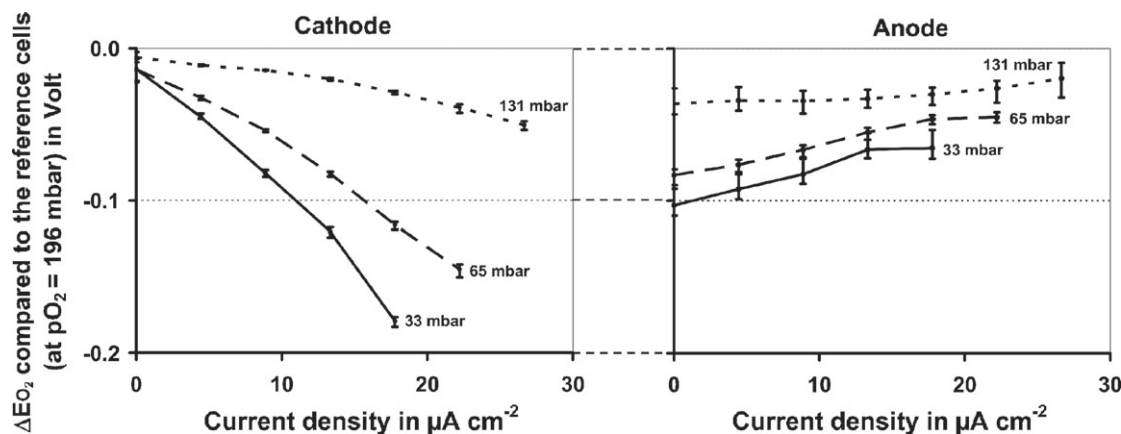

Fig. 10. Effect of oxygen partial pressure on the electrode potentials at different current densities. The oxygen partial pressure in the testing medium is indicated in the figure. The potential values are normalized to the corresponding potentials of three reference fuel cells operated at an oxygen partial pressure 196 mbar. Bars represent maximum and minimum values.

the freshly prepared anodes. Both, the positive shift in open circuit potential and the apparent activation polarization after prolonged operation indicate that degradation at the anode stems from a deactivation of the platinum–bismuth catalyst. A likely explanation for the loss in catalytic activity is the adsorption of glucose oxidation products [41,42].

5.3. Oxygen sensitivity

In Fig. 10 the effect of lower oxygen partial on anode and cathode potential of an operating fuel cell is compared to three reference fuel cells operating at the constant oxygen partial pressure of 196 mbar. At the cathode, a decrease in oxygen partial pressure from 196 to 33 mbar has only a small effect on open circuit potential, amounting to $-(14 \pm 8)$ mV. The corresponding anode open circuit potential shift is approx. sevenfold larger and amounts to $-(103 \pm 9)$ mV. The large negative potential shift at the anode is attributed to a diminished oxygen crossover through the cathode at lower oxygen partial pressures. Consequently the formation of the mixed potential at the anode is less pronounced and the electrode attains a more negative potential closer to the redox potential of glucose oxidation (see also Section 2.1).

Under load the cathode polarization (as compared to the reference cells) increases both, with increasing current density and decreasing oxygen partial pressure. This shows that under reduced oxygen partial pressures mass transfer losses increasingly dominate the cathode reaction. These losses are partly counterbalanced by a more negative anode potential due to diminished oxygen crossover. A change in oxygen partial pressure from 196 to 131 mbar therefore does not lead to a significant change in peak performance of the fuel cells. However, at the lower physiological oxygen partial pressures (65 and 33 mbar, estimated range in body tissue, see Section 4.3) the peak performance is reduced by approximately 20%, as compared to the reference cells operating at an oxygen partial pressure of 196 mbar (data not shown). Also, there is a noticeable negative shift in anode potential when decreasing the oxygen partial pressure from 65 to 33 mbar, amounting to values around 20 mV over the investigated current density range. This shows that even in the relatively low physiological oxygen partial pressure range the reactant separation in the fuel cell is incomplete.

5.4. Glucose sensitivity

The sensitivity of the fuel cells electrode potential to variations in glucose concentration was investigated at a current density of 8.9 μA cm^{-2} and under oxygen partial pressures of 196 and 33 mbar. The cathode potential is not significantly influenced (voltage shift of less than 2 mV, data not shown) by variations in glucose concentration within the investigated range. In contrast, the stepwise increase of glucose concentration results in a negative potential shift at the anode (Fig. 11). Both, at oxygen partial pressures of 196 and 33 mbar this negative potential shift decreases with increasing glucose concentration in the testing solution. The magnitude of the negative potential shift is more pronounced at 196 mbar oxygen partial pressure. Here, the increase in glucose concentration from 3.8×10^{-3} to 5.0×10^{-3} mol L^{-1} (approximate concentration difference between tissue and blood [39]) results in a negative potential shift of $-(131 \pm 22)$ mV. This is almost eight times higher than the negative potential shift of $-(17 \pm 1)$ mV observed at an oxygen partial pressure of 33 mbar. The glucose sensitivity can therefore be explained by the incomplete separation of reactants and the resulting crossover of oxygen to the anode (see also Section 5.2). Both, at lower oxygen partial pressure or higher glucose concentration the oxygen present at the anode is more effectively consumed by a direct chemical reaction with glucose in the outer layers of the
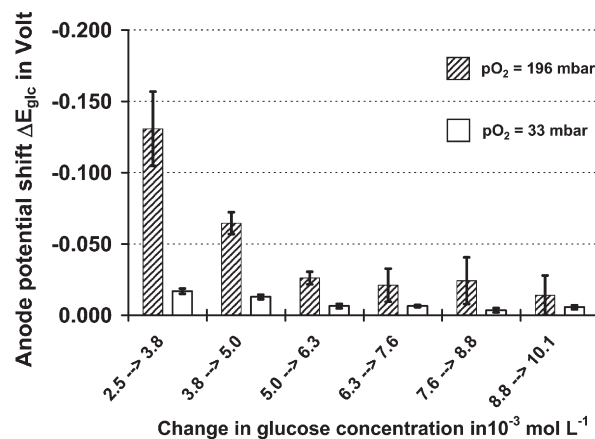

Fig. 11. Effect of glucose concentration increase on the anode potential at a current density of 8.9 μA cm^{-2}, recorded under two different oxygen partial pressures (as indicated in the figure). Given is the average of three parallel experiments, bars represent maximum and minimum values.

anode. The formation of a mixed potential is thereby diminished, and the anode attains a potential closer to the redox potential of glucose oxidation (see also Section 2.1). This explanation is in agreement with Wolfson et al. [24], who found that in the absence of oxygen the glucose oxidation performance of platinum electrodes is not significantly influenced by varying glucose concentrations in the range of 0.05×10^{-3} to 50×10^{-3} mol L^{-1}.

Of particular interest is the performance of the fuel cells when both, the oxygen partial pressure and the glucose concentration resemble the situation in body tissue. This data point is available from the glucose sensitivity experiments conducted at an oxygen partial pressure of 33 mbar and with a glucose concentration of $3.8 \, 10^{-3}$ mol L^{-1} in the testing solution. Under these conditions the fuel cell power density amounts to $(0.74 \pm 0.12) \mu$W cm^{-2} (recorded after a total of 157 days of operation, data not shown). At the same oxygen partial pressure but at the higher glucose concentration of 5×10^{-3} mol L^{-1} the power density is $(0.83 \pm 0.09) \mu$W cm^{-2}, a performance increase of only approx. 13%.

6. Conclusion

Based on the historic publications of Rao et al. [14] we successfully reconstructed a comprehensive manufacturing protocol for abiotically catalyzed glucose fuel cells and characterized their long-term performance in physiological glucose solution. Over a period of 224 days the maximum power density decreased from (3.3 ± 0.2) to $(1.0 \pm 0.05) \mu$W cm^{-2}. This is comparable to the performance reported for similarly constructed fuel cells [14,22].

A novel aspect of the present work is the characterization of fuel cell performance with individually resolved electrode potentials. This technique enables us to show that the major share of overall fuel cell degradation stems from a shift in anode open circuit potential to more positive values. The experimental results indicate that this roots from a gradual deactivation of the platinum–bismuth catalyst, presumably by adsorption of glucose oxidation products. The key challenge for successful long-term application of the technology as sustainable medical implant power supply will therefore be the development of more poisoning-resistant glucose oxidation catalysts. In this context Raney-type catalysts, fabricated from platinum–nickel alloys, have already shown excellent performance [25]. However, from the viewpoint of biocompatibility the use of nickel is problematic and future research will have to concentrate on non-toxic alloying partners.

While less pronounced, cathode degradation is a further aspect to be optimized. Besides a progressing deactivation of the activated carbon catalyst, part of the performance loss can also be attributed to an increasing area specific resistance in the ohmic range. This suggests a progressing loss of electrical contact between the activated carbon particles due to a chemical degradation of the PVA–PAA binder. Improvement can be expected from the application of chemically more stable polymers as well as the construction of binder-less electrodes based on inherently conductive porous substrates.

Besides the time-dependent degradation of anode and cathode, we were able to identify two further factors influencing fuel cell power density. First of all, the reactant separation in the presented fuel cells is not complete, so that under all the investigated operation conditions oxygen reaches to the anode. This leads to the formation of a mixed potential that is more positive than the anode potential in oxygen-free solution. The fuel cell performance might thus be significantly improved by implementing a catalytically active interlayer between the electrodes, where oxygen is consumed by a direct chemical reaction with glucose. The second factor is the mass transfer governed cathode reaction under the relatively low physiological oxygen partial pressures. This limitation might be alleviated by the application of more effective oxygen reduction catalysts that, in contrast to the two-electron pathway observed on carbon materials [43], enable the transfer of four electrons per molecule oxygen. Prime candidates are platinum [44,45] and its alloys that also exhibit a more positive electrode potential upon oxygen reduction [14,46]. Obviously, these catalysts will either have to be selective toward oxygen reduction in the presence of glucose, or protected for instance with a polymer layer that is impermeable to glucose to prevent the formation of a mixed potential at the cathode.

Acknowledgements

References

[1] L. Mateu, F. Moll, Proc. SPIE Int. Soc. Opt. Eng. 5837 (2005) 359–373.
[2] R.A.M. Receveur, F.W. Lindemans, N.F. de Rooij, J. Micromech. Microeng. 17 (2007) R50–R80.
[3] P. Miao, P.D. Mitcheson, A.S. Holmes, E.M. Yeatman, T.C. Green, B.H. Stark, Microsyst. Technol. 12 (2006) 1079–1083.
[4] S.P. Beeby, M.J. Tudor, N.M. White, Meas. Sci. Technol. 17 (2006) R175–R195.
[5] R. Venkatasubramanian, C. Watkins, C. Caylor, G. Bulman, Proceedings of PowerMEMS 2006, Berkeley, USA, 2006, pp. 1–4.
[6] C. Watkins, B. Shen, R. Venkatasubramanian, Proceedings of the 24th International Conference on Thermoelectronics (ICT 2005), Clemson, USA, 2005, pp. 265–267.
[7] F. von Stetten, S. Kerzenmacher, R. Sumbharaju, R. Zengerle, J. Ducrée, Proceedings of the Eurosensors XX Conference 2006, Göteborg, Sweden, 2006, p. M2C-KN.
[8] S. Kerzenmacher, R. Sumbharaju, J. Ducrée, R. Zengerle, F. von Stetten, Transducers '07—Digest of Technical Papers, Lyon, France, 2007, pp. 125–128.
[9] A. Heller, Phys. Chem. Chem. Phys. 6 (2004) 209–216.
[10] R.A. Bullen, T.C. Arnot, J.B. Lakeman, F.C. Walsh, Biosens. Bioelectron. 21 (2006) 2015–2045.
[11] A. Heller, AIChE J. 51 (2005) 1054–1066.
[12] H. Warner, B.W. Robinson, Digest of the 7th International Conference on Medical and Biological Engineering, Stockholm, Sweden, 1967, p. 520.
[13] R.F. Drake, B.K. Kusserow, S. Messinger, S. Matsuda, Trans. Am. Soc. Artif. Int. Organs 16 (1970) 199–205.
[14] J.R. Rao, G. Richter, F. von Sturm, E. Weidlich, Berichte der Bunsen-Gesellschaft (Phys. Chem. Chem. Phys.) 77 (1973) 787–790.
[15] S.K. Wolfson, S.J. Yao, A. Geisel, H.R. Cash, Trans. Am. Soc. Artif. Int. Organs 16 (1970) 193–198.
[16] E. Weidlich, G. Richter, F. von Sturm, J.R. Rao, Biomater. Med. Devices Artif. Organs 4 (1976) 277–306.
[17] Solid state Lithium–Iodine Primary Battery, US Patent 3,660,163 (May 2, 1972).
[18] K. Jeffrey, V. Parsonnet, Circulation 97 (1998) 1978–1991.
[19] W. Greatbat, J.H. Lee, W. Mathias, M. Eldridge, J.R. Moser, A.A. Schneider, IEEE Trans. Biomed. Eng. BM18 (1971) 317.
[20] L.S.Y. Wong, S. Hossain, A. Ta, J. Edvinsson, D.H. Rivas, H. Naas, IEEE J. Solid-State Circuits 39 (2004) 2446–2456.
[21] R. Sarpeshkar, C. Salthouse, J.J. Sit, M.W. Baker, S.M. Zhak, T.K.T. Lu, L. Turicchia, S. Balster, IEEE Trans. Biomed. Eng. 52 (2005) 711–727.
[22] J.R. Rao, G.J. Richter, F. von Sturm, E. Weidlich, Bioelectrochem. Bioenerg. 3 (1976) 139–150.
[23] S. Kerzenmacher, et al., J. Power Sources (2008), doi:10.1016/j.jpowsour.2008.03.31.
[24] S.K. Wolfson, S.L. Gofberg, P. Prusiner, L. Nanis, Trans. Am. Soc. Artif. Int. Organs 14 (1968) 198–203.
[25] U. Gebhardt, J.R. Rao, G.J. Richter, J. Appl. Electrochem. 6 (1976) 127–134.
[26] J.R. Rao, G. Richter, F. von Sturm, E. Weidlich, M. Wenzel, Biomed. Eng. 9 (1974) 98–103.
[27] J.R. Rao, G. Richter, Naturwissenschaften 61 (1974) 200–206.
[28] J.R. Rao, G. Richter, E. Weidlich, F. von Sturm, Phys. Med. Biol. 17 (1972) 738.
[29] Implantable fuel cell, US Patent 3,861,397 (January 21, 1975).
[30] J.R. Rao, in: G. Milazzo, M. Blank (Eds.), Bioelectrochemistry. I. Biological Redox Reactions, Plenum Press, New York, 1983, pp. 283–335.
[31] Method for Preparation of Gluconic Acid by Catalytic Oxidation of Glucose, US Patent 5,132,452 (July 21, 1992).
[32] R.A. Freitas, Nanomedicine, Volume IIA: Biocompatibility, Landes Bioscience, Georgetown, 2003.
[33] G. Paradossi, F. Cavalieri, E. Chiessi, J. Mater. Sci. Mater. Med. 14 (2003) 687–691.
[34] V.P. Shastri, Curr. Pharm. Biotechnol. 4 (2003) 331–337.
[35] G.G. Briand, N. Burford, Chem. Rev. 99 (1999) 2601–2657.
[36] D.A. Gough, F.L. Anderson, J. Giner, C.K. Colton, J.S. Soeldner, Anal. Chem. 50 (1978) 941–944.
[37] N. Chang, W.H. Goodson, F. Gottrup, T.K. Hunt, Ann. Surg. 197 (1983) 470–478.
[38] F. Goda, J.A. Ohara, K.J. Liu, E.S. Rhodes, J.F. Dunn, H.M. Swartz, Oxygen Transport to Tissue XVIII, vol. 411, 1997, pp. 543–549.
[39] D.G. Maggs, R. Jacob, F. Rife, R. Lange, P. Leone, M.J. During, W.V. Tamborlane, R.S. Sherwin, J. Clin. Investig. 96 (1995) 370–377.
[40] A. Hamnett, in: W. Vielstich, A. Lamm, H. Gasteiger (Eds.), Handbook of Fuel Cells—Fundamentals, Technology, Applications, John Wiley & Sons, Ltd., Chichester, England, 2003, pp. 3–12.
[41] M.L.B. Rao, R.F. Drake, J. Electrochem. Soc. 116 (1969) 334–337.
[42] H. Lerner, J. Giner, J.S. Soeldner, C.K. Colton, J. Electrochem. Soc. 126 (1979) 237–242.
[43] E. Yeager, Electrochim. Acta 29 (1984) 1527–1537.
[44] D. Pletcher, S. Sotiropoulos, J. Electroanal. Chem. 356 (1993) 109–119.
[45] Y.J. Li, R. Lenigk, X.Z. Wu, B. Gruendig, S.J. Dong, R. Renneberg, Electroanalysis 10 (1998) 671–676.
[46] A. Kozawa, V.E. Zilionis, R.J. Brodd, J. Electrochem. Soc. 117 (1970) 1470–1474.